ACS OMEGA

Open Access

http://pubs.acs.org/journal/acsodf

Article

Theoretical Understanding of Electromigration-Related Surface Diffusion and Current-Induced Force in Ag−Pd Systems

Yumin Zhang, Zijian Hong, Zhizhen Ye, and Xinhua Pan*

Cite This: *ACS Omega* 2024, 9, 29576−29584

Read Online

ACCESS | Metrics & More | Article Recommendations | Supporting Information

ABSTRACT: Electromigration, as a common reason for interconnect failure, is becoming increasingly important in the ongoing decrease in the integrated circuit manufacturing process. A study is being carried out utilizing the ab initio calculational method to gain a deeper understanding of electromigration, with a focus on the atom diffusion process in the Ag−Pd alloy system, a commonly used interconnect material. We begin by establishing that the primary mechanism of diffusion is step-edge diffusion on the (111) surface. Following this, we examine the current-induced force exerted on the migrating Ag atom. The Pd substitutional defect reveals an effect that increases the energy barrier of diffusion and decreases the current-induced force that powers the directional migration.

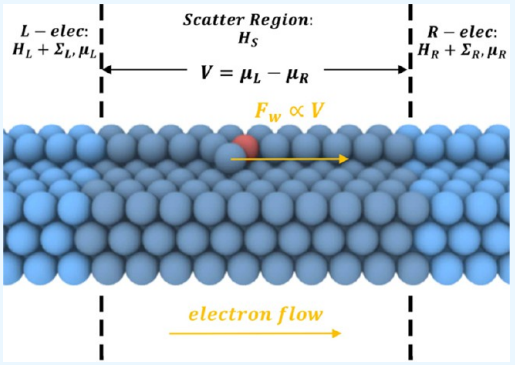

INTRODUCTION

As one of the main failure mechanisms for interconnects, electromigration (EM) has received tremendous attention in the field of integrated circuits. First discovered by Geradin in 1861, EM refers to the motion of atoms in a metal under an external electric field.[1] The driving force for EM has been extensively investigated since the 1960s. The Fiks,[2] Huntington, and Grone[3] ballistic model proposes that the total force is comprised of the following two components: the direct force exerted by the electric field on atomic nuclei and a current-induced wind force resulting from the exchange of momentum between the carrying electrons and the nuclei.

$$Z^* e\vec{E} = \vec{F}_{\text{total}} = \vec{F}_{\text{direct}} + \vec{F}_{\text{wind}} = Z_d e\vec{E} + Z_w e\vec{E} \quad (1)$$

The effective charge, denoted Z^*, is a parameter used to evaluate the EM property. In some cases, when the value of Z_d is relatively small, Z_w is used instead of Z^*. Bosvieux and Friedel[4] suggested that the wind force arose from the polarized electron density around the nuclei. Kumar and Sorbello[5] introduced the linear-response approach. Based on these theories, calculations for Z_w with models consisting of real metallic atoms are mostly done within the Kohn−Korringa−Rostoker (KKR) frame by Duryea and Huntington,[6] Gupta et al.,[7,8] Vanek and Lodder,[9−11] Rous et al.,[12−15] and Dekker et al.,[16,17] most of which obtained quantitatively correct results. More recently, works based on the molecular dynamic method[18] and machine learning method[19] have also been applied in studying the dynamic process of EM or the effective charge Z^*.

Experimentally, EM is observed using the stress test with a higher temperature due to its slow speed in normal conditions, using observation methods like the marker-based motion method.[20,21] There is Black's equation[22] for predicting interconnects' failure time with the result of the stress test. However, Hummel and Geier's study[23] suggests that at a lower temperature (below 225 °C), EM is mainly contributed by surface diffusion with a diffusion barrier of 0.3 eV, while at a higher temperature (above 225 °C), grain boundary transport contributes most with a diffusion barrier of about 0.9 eV. As the interconnect material is unlikely to reach 1000 K during service, the stress test might not be able to reveal the EM under normal service conditions, especially when surface EM plays the main role.

For on-chip interconnects, the scale-down of the chip process leads to a decrease in the cross section of interconnects, which means a higher current density, resulting in a higher wind force and more serious EM. Although some techniques, like the Cu alloy seed layer, are applied to suppress EM, the lifetime of the interconnect is still predicted to be seriously decreased.[24]

Another case is to connect the chip to the external circuit, namely, the integrated circuit packaging, where Ag is used as a cheap substitution for Au, whose wide application is limited by the high and continuously growing price.[25] While Ag features the highest electrical and thermal conductivity among metals,

Received: March 19, 2024
Revised: June 14, 2024
Accepted: June 18, 2024
Published: June 26, 2024

EM has become one of the main problems. In practice, alloying is used to stabilize Ag bonding wires with Pd and Au elements. There have been detailed studies of Ag−Au−Pd[26,27] and Ag−Pd[28,29] systems, where surface diffusion is regarded as the main contributor to EM. Specifically, the study of Ag−Pd systems[28] shows a growth of the surface diffusion barrier from about 0.36 to 0.46 eV, based on a fitting using Black's equation.[22] The surface diffusion barrier increase is also discovered in the Ag−Au−Pd system and seems to be the reason why alloying suppresses EM, as KKR-GF-based calculation shows that the driving force of Pd and Ag atoms is very close in the Pd−Ag alloy system, unlike the case of the Al−Cu system, where the difference in driving force takes effect.[16] However, the surface diffusion mode they refer to is the diffusion of adatom on the Ag(001) face.[30] Although the diffusion barrier is close to the experimental value, the density of the (001) face is rather low due to its high formation energy (∼1 eV). Thus, the surface EM is attributed to a different diffusion mode. There have been KKR-GF-based studies regarding the migration of atoms attached to the step edge as the main contributor to mass transport,[14] and STM observation[31,32] also shows the edge of the Ag(111) surface step to be frizzle, suggesting attached atoms on the step edge. There has also been an EAM-based study[33] that shows the diffusion barrier of such diffusion mode on the Ag(111) surface close to 0.3 eV, providing an excellent starting point for further research.

Although EM is considered a disadvantageous effect for interconnects, it may also be utilized for specific applications. Ohno et al.[34] utilized the surface EM on Ag for the implementation of memristors. Improving these applicational studies also requires a more detailed theoretical study on EM.

In this work, an ab initio study is carried out for the atom diffusion related to the step edge on the Ag(111) face in order to explore the microstructural mechanism of EM. Furthermore, we studied the effect of Pd substitution on the surface EM. Based on the calculational result, we suggest the step-edge diffusion on the Ag(111) surface as the main contributor to the surface electromigration. The Pd substitute suppresses the EM by raising the diffusion barrier and decreasing the current-induced force.

CALCULATION METHODS

Considering that the EM driving force is several orders of magnitude smaller than the chemical bond, we start our work with a series of equilibrium-state calculations to study the surface diffusion mechanism related to EM with a slab model. The calculation is performed using the Vienna Ab initio Simulation Program (VASP).[35] Key parameters including vacuum layer thickness, layer numbers, *k*-point numbers, and ionic step convergence criteria are tested for convergence, as illustrated in Figure S2. In this study, we use a 6 × 6 × 4 slab model (the bottom layer is fixed) with a 12 Å vacuum layer, *γ*-only *k*-point (corresponding to KSPACING = 0.040), cutoff energy of 400 eV (ENCUT = 400), convergence criteria for electronic and ionic steps set as 1×10^{-6} and 3×10^{-2} eV, respectively (EDIFF = 1×10^{-6}, EDIFFG = -3×10^{-2}), and Methfessel−Paxton order 1 smearing method with 0.05 eV smearing width (ISMEA = 1, SIGMA = 0.05). To improve the accuracy of the calculation, especially for the surface system, DFT-D series van der Waals correction[36−39] is incorporated. Several combinations of DFT-D and GGA exchange−correlation functions are tested, and the results are listed in Tables S1 and S2. In general, DFT-D4 improves the accuracy of cohesive energy and force constants over DFT-D3 and GGA only, consistent with the test done by its developer for this metallic system, and is adopted. After initial structural relaxations, CINEB calculations[40,41] are executed to study the energy minimum paths and diffusion barriers.

With the diffusion path determined, we then consider the driving force of EM, the current-induced force, using nonequilibrium Green's function (NEGF)-based codes SIESTA and TRANSIESTA.[42−44] Convergence tests on several key parameters are also conducted, as illustrated in Figure S3. Accordingly, we adopt a DZP orbit with a 50 eV cutoff radius and a mesh cutoff of 200 Ry for a balance between accuracy and efficiency. The basic idea is to take each structural interval obtained from previous equilibrium-state calculations as a scatter region in the NEGF calculation and combine the scatter region with two electrodes with different chemical potentials to form the total device. Such a chemical potential difference leads to current flow across the scatter region. The force is then calculated accordingly by using the Hellmann−Feynman theory. For a more detailed description, the reader is encouraged to go through the corresponding SIESTA and TRANSIESTA literature.[42−44] We also utilize OVITO,[45] VASPKIT,[46] and Atomsk[47] as input file generation and output visualization tools.

RESULTS AND DISCUSSION

With surface diffusion calculations, we come to the following conclusions. The main diffusion mode of Ag's surface EM is step-edge diffusion on the (111) surface in the ⟨110⟩ direction, and the existence of Pd substitutes does not change it.

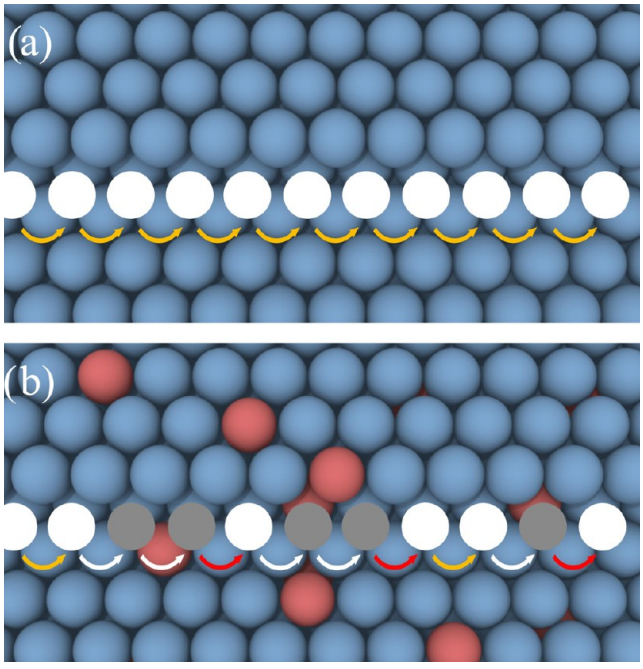

Figure 1. Schematics of a step-edge atom migrating from the left to right by diffusion. Orange arrows represent the diffusion process with an ∼0.33 eV diffusion barrier. White arrows represent diffusion processes with diffusion barriers lower than 0.33 eV, and red ones for diffusion barriers higher than 0.33 eV. (a) Pure Ag system, where white circles represent hollow sites. (b) Ag−Pd system, where Pd substitutes' first neighbor hollow sites are marked with gray circles instead.

https://doi.org/10.1021/acsomega.4c02663
ACS Omega 2024, 9, 29576−29584

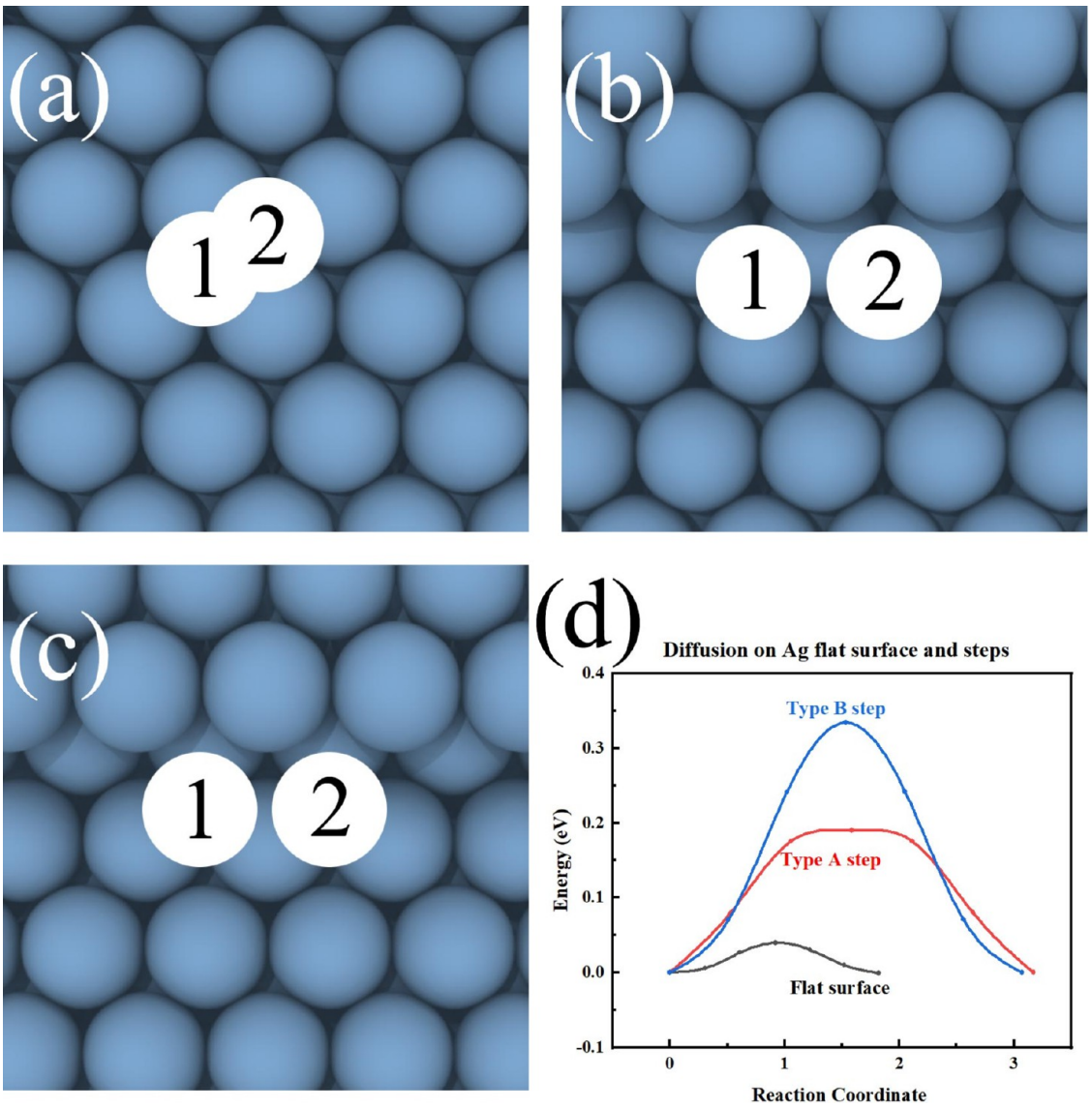

Figure 2. Schematics of the diffusion mechanisms for Ag on the Ag(111) surface of (a) flat, (b) type A step-edge, and (c) type B step-edge surfaces, and the corresponding NEB energy curves in (d). Blue spheres represent Ag atoms, red spheres represent Pd atoms, and white circles with letters represent the start/end positions of diffusion.

Table 1. Diffusion Barriers on Three Surface Structures Corresponding to Figure 2

path	structure (a) (eV)	structure (b) (eV)	structure (c) (eV)
1 → 2	0.06	0.19	0.33
2 → 1	0.06	0.19	0.33

Diffusion barriers do change with Pd substitutes on the surface, as shown in Figure 1. Between two of the Pd substitute's nearest neighbor sites, the diffusion barrier decreases. For diffusion starting from one of Pd's nearest neighbor sites and ending in another hollow site away from Pd, the diffusion barrier increases. Such a change in the diffusion barrier will pin step-edge atoms around Pd substitutes as a mechanism of suppressing EM.

We first consider the self-diffusion of Ag on three different Ag(111) surfaces: A flat surface with a type I step edge and with a type II step edge (Figure 2). On the flat (111) surface, the diffusion barrier for the adatom is found to be 0.06 eV, closely matching the value derived from the earlier literature using EAM-based computational methods.[31] This value is substantially lower than the experimental surface EM barrier for Ag metal (0.3 eV[23]), indicating that diffusion of the adatom on a flat (111) surface is unlikely to be the primary factor contributing to surface EM, while for step-edge diffusion, the calculated diffusion barriers are 0.19 eV along the type A step and 0.33 eV along the type B step, (Table 1)both comparable to the experimental value. Type A and B edges can be found simultaneously on the Ag(111) surface. For instance, an island on the (111) surface has two edges oriented in the ⟨110⟩ direction. Thus, both factors could potentially contribute to the high surface EM barrier.

Next, we examined the effect of the Pd substitute. Here, we focus on configurations involving one (Figure 3) or two (Figure S4) Pd atoms located near the diffusion path. First, in the case of a single Pd substitution, the diffusion barriers between the two nearest neighbors of a Pd atom are smaller compared to that of a Ag atom. This is attributed to the smaller atomic diameter of Pd. The diffusion of atoms away from Pd's nearest neighbor is higher than that of a Ag atom. This is

https://doi.org/10.1021/acsomega.4c02663
ACS Omega 2024, 9, 29576−29584

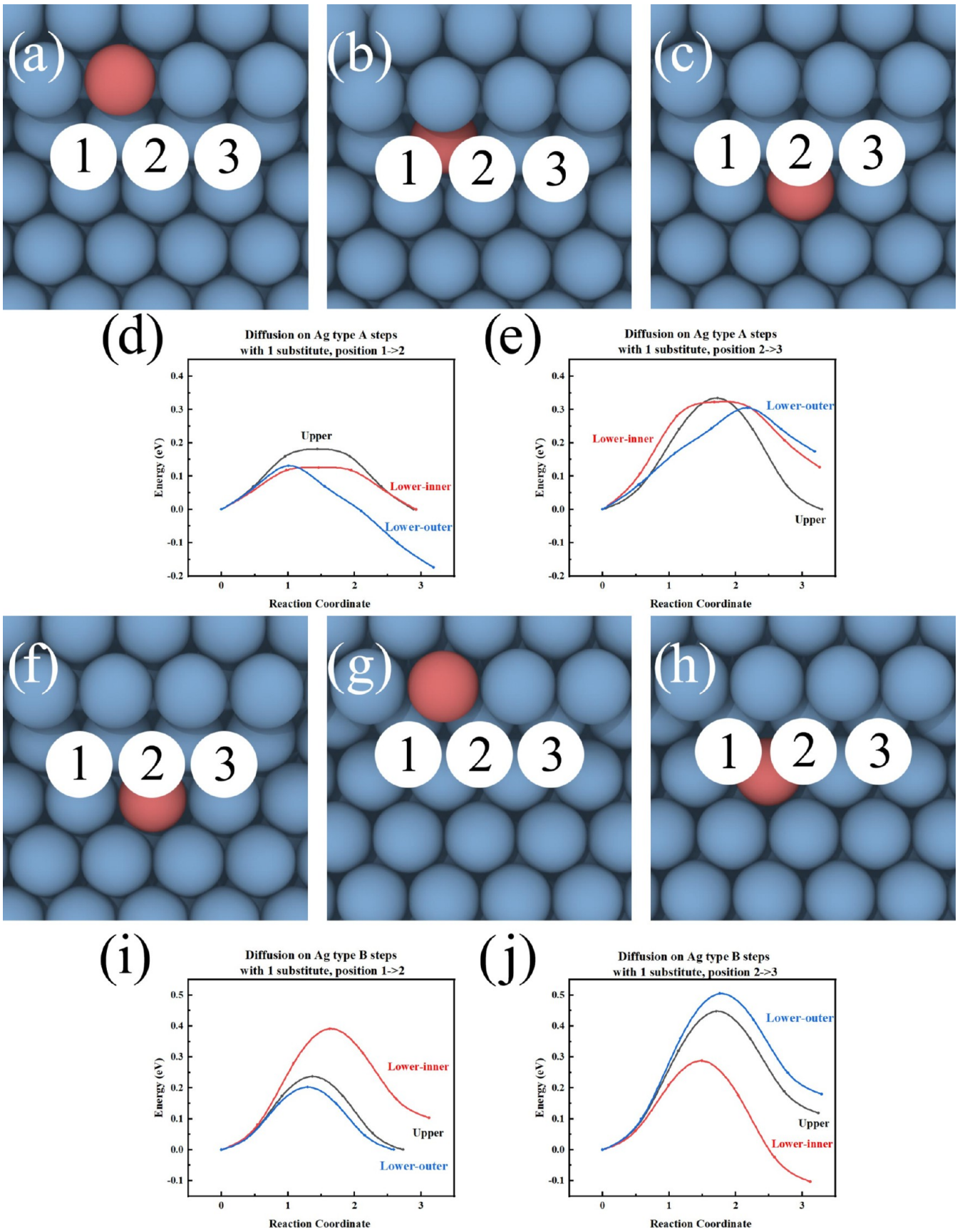

Figure 3. Schematics of the step-edge diffusion mechanisms for Ag atoms on the Ag (111) surface with one Pd substitute on the surface. (a–c) Three cases for type A steps, with corresponding NEB energy curves in (d) and (e). (f–h) 3 Cases for type B steps, with corresponding NEB energy curves in (i, j).

https://doi.org/10.1021/acsomega.4c02663
ACS Omega 2024, 9, 29576–29584

Table 2. Diffusion Barriers of Six Surface Structures Corresponding to Figure 3

path	structure (a) (eV)	structure (b) (eV)	structure (c) (eV)	structure (f) (eV)	structure (g) (eV)	structure (h) (eV)
1 → 2	0.18	0.13	0.13	0.24	0.29	0.20
2 → 1	0.18	0.13	0.31	0.24	0.39	0.20
2 → 3	0.29	0.32	0.31	0.45	0.39	0.50
3 → 2	0.18	0.20	0.13	0.33	0.29	0.32

attributed to the stronger interaction between Ag and Pd than Ag−Ag. Results from cases with two Pd atoms also agree with the above rules. The increase in the potential barrier is determined by the microstructure around the diffusion atoms formed by the Pd substitute. For example, for the type B step, it is generally between 0.06 and 0.17 eV, and some structures can increase the potential barrier by 0.20 eV or higher.(Table 2) Starting from pure Ag, as the Pd content increases, more "traps" are introduced, and more diffusion atoms are "captured." The average electromigration diffusion activation energy increases by about 0.12 eV until all diffusion atoms are "captured." Subsequently, as the Pd content continues to increase, the main effect is to "deepen the trap"; thus, the average EM activation energy increases slowly with the increase of Pd content. Such a trend aligns well with the experimental result.[28] Cases where the Pd substitute has no direct contact with diffusion atoms are also considered, as given in Figure S5. The alteration in the diffusion barrier in this scenario is minimal compared with the case involving direct contact.

The step-edge atom can detach from the step and diffuse like a surface adatom. However, further calculations (Figure 4) indicate that such a process is unlikely to happen. The energy barrier for this detachment process is either significantly higher (0.78 eV) compared to the direct diffusion along the step (0.19 eV) for a type A step, or it increases almost monotonically with a very small backward diffusion barrier (0.02 eV) for a type B step. Additionally, the diffusion barrier between two "detached sites" on a type A step is very close to the adatom on a flat surface (∼0.05 eV). On the other hand, for a type B step, instead of directly moving from one "detached site" to another, the trajectory obtained from the NEB method shows that the diffusing atom first reattaches to the step due to the presence of that small backward diffusion barrier. One may suggest that the presence of a Pd substitute reduces the forward diffusion barrier of the detachment process. This occurs when the two hollow sites of the detachment process are the two nearest neighbors of the Pd substitute atom. The forward diffusion barrier decreases based on the calculation results: for a type A step, it decreases from 0.78 to 0.61 eV; for a type B step, it decreases from 0.48 to 0.41 eV. Nevertheless, the forward barrier remains significantly greater compared to diffusion along the step on a type A step or with the preserved monotonic profile on a type B step. Therefore, the diffusion mode with the Pd substitute will continue to be primarily step-edge diffusion (Table 3).

We proceed to perform the NEGF computation. To start, we examine the force acting on the atom at the step-edge in three directions while varying the potential difference between the two electrodes. The outcome is illustrated in Figure S6. The force−potential relationship exhibits a pronounced linear relationship in the y direction, which runs parallel to the direction of electron transport and possesses a notable slope. The force−potential relation is more unpredictable in the x and z directions, which are perpendicular to the direction of electron transport. In these directions, the change amplitude is 1−2 orders of magnitude smaller compared to the y direction. The calculated current-induced force is primarily in the transport direction with strong force−potential linearity. This finding aligns with the outcomes of a prior calculation[15] and is consistent with the description provided by the ballistic model.

Next, we consider a diffusion path represented by a start, an end, and several (in this case, 5) interval "image" structures given by the previous NEB calculation. Each of the seven structures is treated as a scatter region and combined with the same pair of electrodes to generate seven devices. For each device, calculations are performed with a potential difference ranging from −0.3 to 0.3 V with a 0.1 V step. The force on the step-edge atom along the y direction is then collected. Ultimately, we employed linear regression to establish the relationship between force and potential. Next, we evaluate the slope (dF/dV), as the forces acting on step-edge atoms are typically nonzero in the majority of NEB interval structures. Figure S7 provides an example of this. Given the extensive computational resources needed for NEGF, we restrict our analysis to six diffusion paths: an adatom on a flat surface, a step-edge atom on type A and B steps, and three scenarios using Pd substitution on type B steps, as shown in Figure 5. The average force exerted on a single adatom on a flat surface is found to be 0.146 e/Ang. The average forces per voltage introduced for type A and B step-edge atoms are 0.188 and 0.167 e/Ang, respectively, approximately 1.2 times higher than the force value for surface adatoms. A similar relationship that step-edge atom experiences a slightly higher than flat surface adatom was also observed on the Cu(001) surface by Rous.[14] If we assume that the potential drop is identical in the y direction, we obtain a Z_w value of −9.73 or −8.65. Previous calculations have yielded a wide range of Z_w values, ranging from −3.3[16] to −36.5.[11,48] Experimental results have also produced diverse values of −5.1,[19] −6.8,[48] and −19.9.[49] While it is true that the voltage gradient along the y direction is not constant due to the presence of step-edge atoms, this comparison demonstrates that our calculations yield rather reasonable results. All force-diffusion coordinate curves exhibit symmetry, displaying an increase in force near the saddle point of diffusion. This observation aligns with the findings on the Cu(001) surface.[14] The inclusion of a Pd replacement results in a reduction in force, as evidenced by the average force per voltage value of 0.126 e/Ang for the diffusion path depicted in Figure 4d, representing a decrease of approximately 25%. Such a decrease can be attributed to the differences in the electronic structures of Pd and Ag atoms, with the former one lacking a 5s electron, resulting in a lower local charge density and consequently current density near the step-edge atom. Unfortunately, the current SIESTA and TRANSIESTA codes lack the capability to provide us with the local current value. This value is related to the imaginary component of the nonequilibrium density matrix, which is disregarded.[44] As the step-edge atom moves away and decouples with the Pd substitute, the force exerted increases, and the value reverts

https://doi.org/10.1021/acsomega.4c02663
ACS Omega 2024, 9, 29576−29584

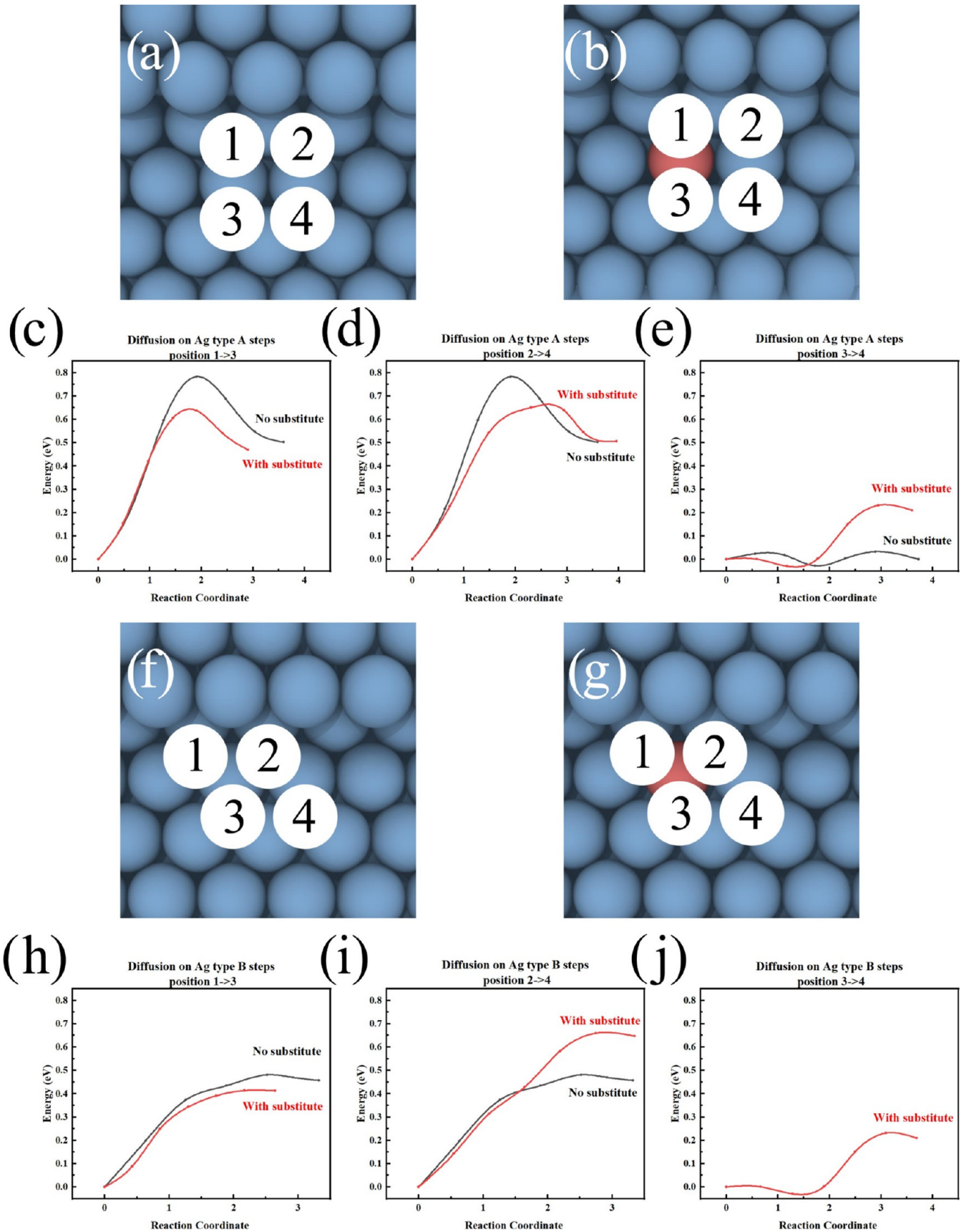

Figure 4. Schematics of the detach process of step-edge Ag atoms on Ag(111) surfaces. (a, b) Type A steps, with corresponding NEB energy curves in (c−e). (f) and (g) Type B steps, with corresponding NEB energy curves in (h−j).

https://doi.org/10.1021/acsomega.4c02663
ACS Omega 2024, 9, 29576−29584

Table 3. Diffusion Barriers of Six Surface Structures Corresponding to Figure 4

path	structure (a) (eV)	structure (b) (eV)	structure (f) (eV)	structure (g) (eV)
1 → 3	0.78	0.61	0.48	0.41
3 → 1	0.28	0.14	0.02	0.00
2 → 4	0.78	0.65	0.48	0.66
4 → 2	0.28	0.15	0.02	0.01
3 → 4	0.06	0.26		0.27
4 → 3	0.06	0.02		0.03

back to that of a typical type B step. When the Pd substitute is placed below the surface without direct contact with diffusing Ag, like the case depicted in Figure 5e/f, the average force per voltage is 0.158 e/Ang. The decrease in force is only one-fourth of the decrease observed in the direct contact case. This indicates that the impact of Pd substitution on reducing the current-induced force is comparable to that of increasing the diffusion barrier, as the effect is only significant when there is direct contact between Pd and the diffusion atom (Tables 4 and 5).

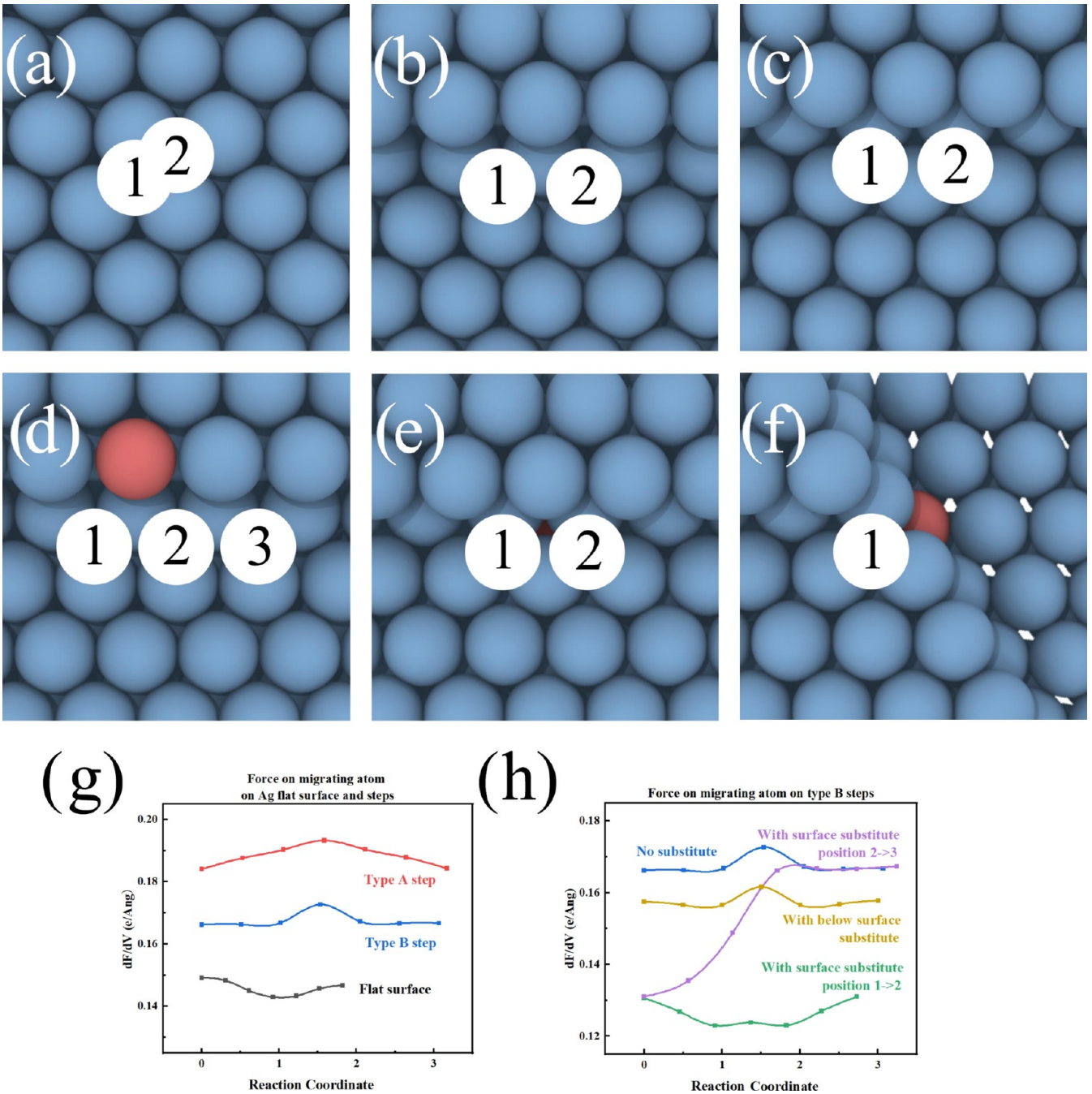

Figure 5. Schematics of calculation on current-induced force along the diffusion paths of Ag atoms on Ag(111) surfaces. (a−c) Three diffusion paths for migrating atoms on the flat surface, type A steps, and type B steps, with the corresponding current-induced force in (g). (d−f): Two diffusion paths for migrating atoms on type B steps with different Pd substitution structures, with corresponding current-induced force in (h). For the atomic structure in (e), where the Pd substitute is placed in the layer below the surface, some atoms are removed for a clearer view, as shown in (f).

https://doi.org/10.1021/acsomega.4c02663
ACS Omega 2024, 9, 29576−29584

Table 4. Force Per Voltage on Migrating Ag Atoms at Different Interval Positions along Three Paths Corresponding to Figure 5g[a]

NEB image	structure (a) (e/Å)	structure (b) (e/Å)	structure (c) (e/Å)
00	0.1491	0.1841	0.1662
01	0.1482	0.1876	0.1662
02	0.1450	0.1903	0.1668
03	0.1430	0.1932	0.1727
04	0.1433	0.1903	0.1673
05	0.1457	0.1878	0.1666
06	0.1467	0.1843	0.1667

[a]NEB image 00−06 corresponds to seven points on each of the three curves.

Table 5. Force Per Voltage on Migrating Ag Atoms at Different Interval Positions along the Last Three Paths Corresponding to Figure 5h[a]

NEB image	structure (b) 1 → 2 (e/Å)	structure (b) 2 → 3 (e/Å)	structure (c) (e/Å)
00	0.1307	0.1310	0.1575
01	0.1268	0.1355	0.1566
02	0.1230	0.1489	0.1565
03	0.1238	0.1661	0.1616
04	0.1230	0.1667	0.1566
05	0.1270	0.1666	0.1568
06	0.1310	0.1673	0.1578

[a]NEB image 00−06 corresponds to seven points on each of the last three curves.

Although the NEGF code does not provide information about the real-space-resolved local current density, it does allow us to determine the total current flowing through the device. The $I-V$ characteristics of the three structures are analyzed as the final part of the NEGF calculation. These structures include a type B edge without a step-edge atom, a type B edge with a step-edge atom, and a type B edge with both a Pd substitution and a step-edge atom. The analysis is depicted in Figure S8. In all three situations, the device demonstrates linear resistance, and the inclusion of a step-edge atom reduces the current by introducing additional resistance. The introduction of a Pd substitution has a minimal impact on the overall conductivity, unlike that in the case of a bulk alloy under these precise conditions.

The process of step-edge diffusion on the Ag(111) surface is investigated using the ab initio calculation approach. The findings, when considered alongside existing literature studies,[23,31,32] indicate that step-edge diffusion on the (111) surface is a significant contributor to Ag surface electromigration. Pd substitutional defect raises the diffusion barrier of 0.05−0.2 eV as one mechanism of suppressing surface electromigration. The current-induced force along the diffusion path determined is then studied by NEGF calculation, which gives results that are consistent with previous calculations.[14,15] Pd substitution decreases the force exerted on migrating atoms with direct contact by about 25%. The effects of both increasing diffusion barriers and decreasing current-induced force are significant under the conditions when Pd substitutes directly contact the diffusion atom. Therefore, it would be advantageous to confine the use of Pd replacement to the vicinity of the surface for application purposes.

■ ASSOCIATED CONTENT

Supporting Information

The Supporting Information is available free of charge at https://pubs.acs.org/doi/10.1021/acsomega.4c02663.

Tests on DFT-D4 (Tables S1 and S2); convergence tests (Figures S2 and S3); verifications of the NEGF method in calculating EM (Figures S6 and S7); some more calculation results on surface diffusion (Figures S4 and S5 and Tables S3 and S4); and other data for reference (Figure S1) (PDF)

■ AUTHOR INFORMATION

Corresponding Author

Xinhua Pan − *School of Materials Science and Engineering, Zhejiang University, Hangzhou 310027, P. R. China; Wenzhou Key Laboratory of Novel Optoelectronic and Nano Materials, Institute of Wenzhou, Zhejiang University, Wenzhou 325006, P. R. China;* orcid.org/0000-0002-0308-3783; Email: panxinhua@zju.edu.cn

Authors

Yumin Zhang − *School of Materials Science and Engineering, Zhejiang University, Hangzhou 310027, P. R. China*

Zijian Hong − *School of Materials Science and Engineering, Zhejiang University, Hangzhou 310027, P. R. China;* orcid.org/0000-0002-3491-0884

Zhizhen Ye − *School of Materials Science and Engineering, Zhejiang University, Hangzhou 310027, P. R. China; Wenzhou Key Laboratory of Novel Optoelectronic and Nano Materials, Institute of Wenzhou, Zhejiang University, Wenzhou 325006, P. R. China;* orcid.org/0000-0002-0886-0115

Complete contact information is available at: https://pubs.acs.org/10.1021/acsomega.4c02663

Notes

The authors declare no competing financial interest.

■ ACKNOWLEDGMENTS

This work was supported by the National Natural Science Foundation of China (Grant No. U22A20133) and the Key Research and Development Program of Zhejiang Province (2021C01030).

■ REFERENCES

(1) Ho, P. S.; Kwok, T. Electromigration in Metals. *Rep. Prog. Phys.* **1989**, *52* (3), No. 301, DOI: 10.1088/0034-4885/52/3/002.

(2) Fiks, V. B. On the Mechanism of the Mobility of Ions in Metals. *Sov. Phys.-Solid State* **1959**, *1* (1), 14−28.

(3) Huntington, H. B.; Grone, A. R. Current-Induced Marker Motion in Gold Wires. *J. Phys. Chem. Solids* **1961**, *20* (1−2), 76−87.

(4) Bosvieux, C.; Friedel, J. Sur Leelectrolyse des Alliages Metalliques. *J. Phys. Chem. Solids* **1962**, *23*, 123−136.

(5) Kumar, P.; Sorbello, R. S. linear Response Theory of Driving Forces for Electromigration. *Thin Solid Films* **1975**, *25* (1), 25−35.

(6) Duryea, T. W.; Huntington, H. B. The Driving Force for Electromigration of An Atom Adsorbed on Simple Metal-Surface. *Surf. Sci.* **1988**, *199* (1−2), 261−281.

(7) Gupta, R. P. Theory of Electromigration in Noble and Transition-Metals. *Phys. Rev. B* **1982**, *25* (8), 5188−5196.

(8) Gupta, R. P.; Serruys, Y.; Brebec, G.; Adda, Y. Calculation of the Effective Valence for Electromigration in Niobium. *Phys. Rev. B* **1983**, *27* (2), 672−677.

(9) Vanek, J.; Lodder, A. Electromigration in Transition-Metals. 1. Computational Method. *J. Phys.: Condens. Matter* **1991**, *3* (38), 7307−7330.
(10) Vanek, J.; Lodder, A. Electromigration in Transition-Metals. 2. Light Interstitials in Cu, Ag, Ni, Pd, Al, V, Nb and Ta. *J. Phys.: Condens. Matter* **1991**, *3* (38), 7331−7361.
(11) Vanek, J.; Lodder, A. Electromigration in Transition-Metals. 3. Substitutional Impurities in Cu, Ag, Al and Nb. *J. Phys.: Condens. Matter* **1991**, *3* (43), 8403−8416.
(12) Rous, P. J. Electromigration Wind Force at Stepped Al Surfaces. *Phys. Rev. B* **1999**, *59* (11), 7719−7723.
(13) Rous, P. J. Multiple-Scattering Theory of the Surface Resistivity of Stepped Al Surfaces. *Phys. Rev. B* **2000**, *61* (12), 8484−8488.
(14) Rous, P. J. Theory of Surface Electromigration on Heterogeneous Metal Surfaces. *Appl. Surf. Sci.* **2001**, *175*−*176*, 212−217.
(15) Rous, P. J.; Einstein, T. L.; Williams, E. D. Theory of Surface Electromigration on Metals: Application to Self-Electromigration on Cu(111). *Surf. Sci.* **1994**, *315* (1), L995−L1002.
(16) Dekker, J. P.; Lodder, A.; Van, E. J. Theory for the Electromigration Wind Force in Dilute Alloys. *Phys. Rev. B* **1997**, *56* (19), 12167−12177.
(17) Dekker, J. P.; Lodder, A. Calculated Electromigration Wind Force in Face-Centered-Cubic and Body-Centered-Cubic Metals. *J. Appl. Phys.* **1998**, *84* (4), 1958−1962.
(18) Xu, D. E.; Hook, M. D.; Mayer, M. In *Molecular Dynamics Study of Nano-scale Ag Surface Electromigration and Effect of Pd Coating Layer*, EEE 14th International Conference On Nanotechnology (IEEE-NANO); IEEE, 2014; pp 640−644.
(19) Liu, Y. C.; Afflerbach, B.; Jacobs, R.; Lin, S. K.; Morgan, D. Exploring effective charge in electromigration using machine learning. *MRS Commun.* **2019**, *9* (2), 567−575.
(20) Ho, P. S.; Huntington, H. B. Electromigration and Void Observation in Silver. *J. Phys. Chem. Solids* **1966**, *27* (8), 1319−1329.
(21) Patil, H. R.; Huntington, H. B. Electromigration and Associated Void Formation in Silver. *J. Phys. Chem. Solids* **1970**, *31* (3), 463−474.
(22) Black, J. R. Electromigration—A Brief Survey and Some Recent Results. *IEEE Trans. Electron Devices* **1969**, *16* (4), 338−347.
(23) Hummel, R. E.; Geier, H. J. Activation Energy for Electrotransport in Thin Silver and Gold-Films. *Thin Solid Films* **1975**, *25* (2), 335−342.
(24) Zhao, W. S.; Zhang, R.; Wang, D. W. Recent Progress in Physics-Based Modeling of Electromigration in Integrated Circuit Interconnects. *Micromachines* **2022**, *13* (6), No. 883, DOI: 10.3390/mi13060883.
(25) https://www.nasdaq.com/market-activity/commodities/gc:cmx.
(26) Guo, R.; Gao, L. M.; Li, M.; Mao, D. L.; Qian, K. Y.; Chiu, H. Microstructure Evolution of Ag-8Au-3Pd Alloy Wire During Electromigration. *Mater. Charact.* **2015**, *110*, 44−51.
(27) Hsueh, H. W.; Hung, F. Y.; Lui, T. S. A Study on Electromigration-Inducing Intergranular Fracture of Fine Silver Alloy Wires. *Appl. Phys. Lett.* **2017**, *110* (3), No. 031902.
(28) Chuang, T. H.; Chen, C. H. Mechanism of The Electromigration In Ag-Pd Alloy Bonding Wires. *Metall. Mater. Trans. A* **2018**, *49* (11), 5904−5910.
(29) Chen, C. H.; Lee, P. I.; Chuang, T. H. Microstructure Evolution and Failure Mechanism of Electromigration in Ag-Alloy Bonding Wire. *J. Alloys Compd.* **2022**, *913*, No. 165266.
(30) Papanicolaou, N. I.; Evangelakis, G. A.; Kallinteris, G. C. Molecular Dynamics Description of Silver Adatom Diffusion on Ag(100) and Ag(111) Surfaces. *Comput. Mater. Sci.* **1998**, *10* (1−4), 105−110.
(31) Poensgen, M.; Wolf, J. F.; Frohn, J.; Giesen, M.; Ibach, H. Step Dynamics on Ag(111) and Cu(100) Durfaces. *Surf. Sci.* **1992**, *274* (3), 430−440.
(32) Wolf, J. F.; Vicenzi, B.; Ibach, H. Step Roughness on Vicinal Ag(111). *Surf. Sci.* **1991**, *249* (1−3), 233−236.
(33) Nelson, R. C.; Einstein, T. L.; Khare, S. V.; Rous, P. J. Energies of Steps, Kinks, and Defects on Ag(100) and Ag(111) Using the Embedded-Atom Method, and Some Consequences. *Surf. Sci.* **1993**, *295* (3), 462−484.
(34) Ohno, T.; Hasegawa, T.; Tsuruoka, T.; Terabe, K.; Gimzewski, J. K.; Aono, M. Short-term Plasticity and Long-term Potentiation Mimicked in Single Inorganic Synapses. *Nat. Mater.* **2011**, *10* (8), 591−595.
(35) Hafner, J.; Kresse, G. The Vienna Ab-Initio Simulation Program VASP: An Efficient and Versatile Tool for Studying the Structural, Dynamic, and Electronic Properties of Materials. In *Properties of Complex Inorganic Solids*; Springer US: Boston, MA, 1997; pp 69−82.
(36) Grimme, S.; Antony, J.; Ehrlich, S.; Krieg, H. A Consistent and Accurate Ab Initio Parametrization of Density Functional Dispersion Correction (DFT-D) for the 94 Elements H-Pu. *J. Chem. Phys.* **2010**, *132* (15), No. 154104.
(37) Grimme, S. Density Functional Theory with London Dispersion Corrections. *WIREs Comput. Mol. Sci.* **2011**, *1* (2), 211−228.
(38) Caldeweyher, E.; Ehlert, S.; Hansen, A.; Neugebauer, H.; Spicher, S.; Bannwarth, C.; Grimme, S. A Generally Applicable Atomic-Charge Dependent London Dispersion Correction. *J. Chem. Phys.* **2019**, *150* (15), No. 154122.
(39) Caldeweyher, E.; Mewes, J. M.; Ehlert, S.; Grimme, S. Extension and Evaluation of the D4 London-Dispersion Model for Periodic Systems. *Phys. Chem. Chem. Phys.* **2020**, *22* (16), 8499−8512.
(40) Henkelman, G.; Jónsson, H. Improved Tangent Estimate in the Nudged Elastic Band Method for Finding Minimum Energy Paths and Saddle Points. *J. Chem. Phys.* **2000**, *113* (22), 9978−9985.
(41) Henkelman, G.; Uberuaga, B. P.; Jónsson, H. A Climbing Image Nudged Elastic Band Method for Finding Saddle Points and Minimum Energy Paths. *J. Chem. Phys.* **2000**, *113* (22), 9901−9904.
(42) José, M. S.; Emilio, A.; Julian, D. G.; Alberto, G.; Javier, J.; Pablo, O.; Daniel, S. P. The SIESTA Method for Ab Initio Order-N Materials Simulation. *J. Phys.: Condens.Matter* **2002**, *14* (11), No. 2745, DOI: 10.1088/0953-8984/14/11/302.
(43) Papior, N.; Lorente, N.; Frederiksen, T.; García, A.; Brandbyge, M. Improvements on Non-Equilibrium and Transport Green Function Techniques: The Next-Generation TRANSIESTA. *Comput. Phys. Commun.* **2017**, *212*, 8−24.
(44) Brandbyge, M.; Mozos, J. L.; Ordejón, P.; Taylor, J.; Stokbro, K. Density-Functional Method for Nonequilibrium Electron Transport. *Phys. Rev. B* **2002**, *65* (16), No. 165401.
(45) Stukowski, A. Visualization and Analysis of Atomistic Simulation Data with OVITO−the Open Visualization Tool. *Modell. Simul. Mater. Sci. Eng.* **2010**, *18* (1), No. 015012, DOI: 10.1088/0965-0393/18/1/015012.
(46) Wang, V.; Xu, N.; Liu, J. C.; Tang, G.; Geng, W. T. VASPKIT: A User-Friendly Interface Facilitating High-Throughput Computing and Analysis Using VASP Code. *Comput. Phys. Commun.* **2021**, *267*, No. 108033.
(47) Hirel, P. Atomsk: A Tool for Manipulating and Converting Atomic Data Files. *Comput. Phys. Commun.* **2015**, *197*, 212−219.
(48) Sorbello, R. S. Theory of Electromigration. *Solid State Phys.* **1998**, *51*, 159−231.
(49) Doan, N. V.; Brebec, G. Electromigration in Non-Dilute Binary-Alloys. *J. Phys. Chem. Solids* **1974**, *35* (2), 141−143.

https://doi.org/10.1021/acsomega.4c02663
ACS Omega 2024, 9, 29576−29584